Photofragmentation of tetrahydrofuran molecules in the vacuum-ultraviolet region via superexcited states studied by fluorescence spectroscopy

Tomasz J. Wasowicz,[1] Antti Kivimäki,[2,3] Marcin Dampc,[1] Marcello Coreno,[2,4] Monica de Simone,[2,3] and Mariusz Zubek[1]

[1]*Department of Physics of Electronic Phenomena, Gdańsk University of Technology, PL-80233 Gdańsk, Poland*

[2]*Gas Phase Beamline@Elettra, Basovizza Area Science Park, I-34149 Trieste, Italy*

[3]*CNR-IOM, Laboratorio Nazionale TASC, I-34149 Trieste, Italy*

[4]*CNR-IMIP, Monterotondo, I-00016 Rome, Italy*

(Received 6 December 2010; published 14 March 2011)

Photofragmentation of tetrahydrofuran molecules in the vacuum-ultraviolet region, producing excited atomic and molecular fragments, has been studied over the energy range 14–68 eV using photon-induced fluorescence spectroscopy. Excited hydrogen atoms H(n), $n = 3$–11, have been detected by observation of the H_α to H_i lines of the Balmer series. The diatomic CH($A^2\Delta$), CH($B^2\Sigma^-$) and $C_2(d^3\Pi_g)$ fragments, which are excited to low vibrational and high rotational levels are identified by their $A^2\Delta \rightarrow X^2\Pi_r$, $B^2\Sigma^- \rightarrow X^2\Pi_r$ and $d^3\Pi_g \rightarrow a^3\Pi_u$ emission bands, respectively. Dissociation efficiency curves for CH($A^2\Delta$) and H(n), $n = 3$–7, have been obtained in the photon energy ranges from their appearance thresholds up to 68 eV. The appearance energies for CH($A^2\Delta$) and H(n), $n = 3$–7, have been determined and are compared with estimated fragmentation energy limits in order to discuss the possible fragmentation processes. In the present studies, superexcited states of tetrahydrofuran are found, which dissociate into the above excited atomic and molecular fragments.

DOI: 10.1103/PhysRevA.83.033411 PACS number(s): 33.80.Gj, 33.50.Dq

I. INTRODUCTION

Dissociation and fragmentation of molecules are produced by absorption of radiation or by collisions with charged particles. In the transfer of energy, the target molecule may be excited to a superexcited state lying above the first ionization potential. Molecules in superexcited states in general decay in a nonradiative way, either by dissociation into neutral fragments or by autoionization. The autoionization process can be readily studied using photoion spectroscopy, while dissociation into neutral fragments is more difficult to investigate experimentally. Nevertheless, if one of the neutral atomic or molecular fragments is formed in an excited state, this dissociation process may be explored using the fluorescence spectroscopy technique, which detects emitted fluorescence.

In recent years, much attention has been paid to the study of nonradiative deactivation of the $\pi\sigma^*$ and $n\sigma^*$ excited states of heteroaromatic molecules, in particular those built with hydroxyl (OH) and azine (NH) groups (e.g., phenol, indole, and pyrrole) [1–7]. The $\pi\sigma^*$ and $n\sigma^*$ general terms designate excited states which are formed by the promotion of an electron from occupied bonding π or nonbonding n orbitals to antibonding σ^* molecular orbitals. The $\pi\sigma^*$ excited states have, in general, small transition dipole moments in the decay to their ground states and repulsive potential energy curves along the OH or NH stretching coordinates. These studies show that the $\pi\sigma^*$ states usually decay by the X-H (X = O, N, S) bond fission, which for five-membered heterocyclic molecules is one of the most efficient decay channels [1–6]. The $\pi\sigma^*$ states can also deexcite by nonradiative transfer to the ground state through a conical intersection between potential energy surfaces [7]. Because of this specific character of the $\pi\sigma^*$ states, experimental investigations of fragmentation dynamics are difficult even when modern experimental methods such as photofragment translational spectroscopies (e.g., photofragment velocity map imaging) are used [7]. These fragmentation dynamics have been examined in quantum-mechanical calculations by analysis of the molecular relaxation processes following, for example, photoexcitation [2].

The tetrahydrofuran (THF) molecule, C_4H_8O, is a cyclic ether (Fig. 1) and may be considered a hydrogenated form of furan. Its interaction with radiation has recently generated a lot of interest among research groups. The five-membered ring of THF is incorporated in the deoxyribose sugar of DNA and links the nucleic bases (adenine, cytosine, guanine, and thymine) with the phosphate groups. As a result, THF is often considered a simple analog of the deoxyribose ring in DNA for investigations of radiation interactions with DNA. The interaction of ionizing radiation with biological material, for example in radiodiagnostic examinations or in medical radiotherapy, produces structural and chemical modifications by bond cleavages in the DNA helix. These modifications originate from the interaction of the primary radiation and secondary species that are produced, such as chemically active secondary radicals. Therefore, to characterize these mechanisms it is important to explore the processes of photodissociation and photofragmentation of components of DNA. The present studies identify dissociation channels in THF, an analog of the DNA structural units, which involve initial excitation into higher-lying superexcited states.

Earlier investigations of the fragmentation of THF concentrated on thermal decomposition and photolysis which lead to stable products in their electronic ground states. In the studies of the thermal decomposition of THF, Klute and Walters [8] detected ethylene and carbon monoxide molecules as the most abundant products, accompanied by methane, ethane, and hydrogen molecules. Pyrolysis of THF molecules was also investigated by Lifshitz *et al.* [9], who used a single-pulse shock tube over the temperature range 1070–1530 K. Two main

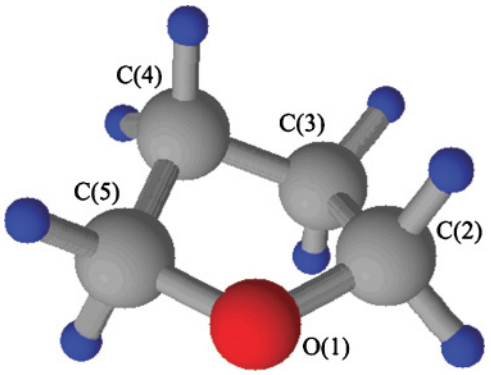

FIG. 1. (Color online) Schematic diagram of the THF molecule, C_4H_8O, in the C_2 (twisted) conformation showing labeling of the atoms. Carbon atom, gray; oxygen atom, red; and hydrogen atom, dark blue.

channels for decomposition were suggested, both producing aldehydes:

$$C_4H_8O \rightarrow CH_2{=}CH_2 + CH_2\text{-}CH_2\text{-}O \text{ and}$$
$$C_4H_8O \rightarrow CH_2\text{-}CH_2\text{-}CH_2 + H_2C{=}O. \quad (1)$$

In the first reaction, the ethylene $CH_2{=}CH_2$ molecule is formed by cleavage of the tetrahydrofuran ring at the C(2)-C(3) and C(4)-C(5) bonds. It was also argued [9] that allene, C_3H_4, and methylacetylene, C_3H_4, formed from propylene, C_3H_6, preserve the original skeleton of THF. In the studies of photolysis of THF, Kramer [10], who used a pulsed CO_2 laser technique, considered initial C-O bond cleavage leading to the transient 1,5-diradical $\cdot CH_2\text{-}CH_2\text{-}CH_2\text{-}CH_2\text{-}O\cdot$, which further decomposes into the fragments of reactions (1). It was also shown [10] that the trimethylene diradical, $\cdot CH_2CH_2CH_2\cdot$, either rearranges to form cyclopropane or propylene, whereas the transient molecule CH_2CH_2O, after isomerization to acetaldehyde, undergoes further decomposition to the methyl CH_3 and formyl CHO radicals. Scala and Rourke [11] indicated that, in the photolysis of THF and its methyl-substituted derivatives at 147.0 nm, the fragmentation of these molecules is initiated by the C-O bond cleavage. More recently, Scala *et al.* [12], using a femtosecond resolved mass spectrometry technique, studied the dynamics of fragmentation reactions of cyclic ethers including THF. They observed that the diradical intermediates and their β cleavages involve simultaneous C-C, C-H σ-bond breakages and C-O, C-C π-bond formations. To compare with experiment, they also presented density-functional-theory calculations of the potential energy surfaces involved and the distributions of the products. In the most recent work, Lee [13] investigated the photodissociation of THF at 193.3 nm using photofragment translational spectroscopy and direct vacuum-ultraviolet (VUV) photoionization. He found that it proceeds mainly on the ground-state potential energy surface following ring opening and efficient internal conversions from the excited to the ground state. This author showed that the $\cdot CH_2\text{-}CH_2\text{-}CH_2\text{-}CH_2\text{-}O\cdot$ diradical decomposes by scission of the C(1)-C(2), C(2)-C(3), and C(1)-H bonds, yielding fragments of reactions (1). It was also shown that hydrogen transfer from the C(3) to the C(1) atom competes with direct fragmentation of the diradical and leads to formation of CH_2OH. Apart from the above fragments, SenGupta *et al.* [14] observed a reaction channel leading to the occurrence of the OH radical in a recent photodissociation study. The proposed dissociation mechanism involves cleavage of the C-O bond, hydrogen migration from C(2) to O(1), and the C-OH bond scission directly producing the OH fragment [14].

In the present work, we have investigated photofragmentation processes of THF that lead to excited hydrogen atoms H(n), $n = 3$–11, and excited diatomic CH($A^2\Delta$), CH($B^2\Sigma^-$), and $C_2(d^3\Pi_g)$ fragments in the VUV energy range of 14–68 eV, using photon-induced fluorescence spectroscopy (PIFS) [15]. These atomic and molecular products differ from those previously reported for THF. Dissociation efficiency curves for CH($A^2\Delta$) and H(n), $n = 3$–7, deduced from emission yields were obtained as a function of incident photon energy. Superexcited states of THF occurring in the energy region above 15 eV and which dissociate into the above fragments were identified and are discussed in detail. The appearance energies (AEs) of the CH($A^2\Delta$) and H(n), $n = 3$–7, have also been determined and are compared with estimated fragmentation energy limits to elucidate possible fragmentation processes.

II. EXPERIMENT

The experiments were performed at the Gas Phase Photoemission beamline at the Elettra storage ring in Trieste, Italy. The beamline was described in detail previously [16]. Briefly, synchrotron radiation emitted from an undulator is monochromatized by a spherical grating monochromator that is equipped with a planar premirror. The operational range from 13.6 to 900 eV of the beamline is covered by five interchangeable gratings. For the photon energy range 20–65 eV, the spherical grating used was calibrated by observation positions of resonances in helium double excitation [17] in the first and second orders as well as in neon double excitation [18] in the first order. The low-energy grating was used up to 20 eV photon energy, which was calibrated to within ± 10 meV by measuring the total ion yield of nitrogen and comparing the observed positions of the autoionizing states with the results from Refs. [19–21].

Figure 2 shows the top view of the experimental setup of PIFS. The THF molecular beam emanating from a capillary needle was crossed by the photon beam at the center of the vacuum chamber. Light emitted in the horizontal direction was reflected and collimated by an aluminum spherical mirror in the direction parallel to the electric vector of the incident radiation. The position of the mirror was adjusted by optimizing the observed light intensity. Although the emitted light is collected from a narrower viewcone, the angular distribution of the emission in the present measurements is expected to be isotropic, which would not introduce angular-distribution effects. The collimated light beam left the vacuum chamber via a quartz exit window and was focused onto the entrance slit of the Minuteman 305 MV fluorescence spectrograph. It was next dispersed by a 1200 lines/mm grating, blazed at 500 nm and detected by a CCD detector (Princeton 10:100B), which was cooled by liquid nitrogen. The intensity of the incident photon beam was monitored by a moveable photodiode mounted on a manipulator.

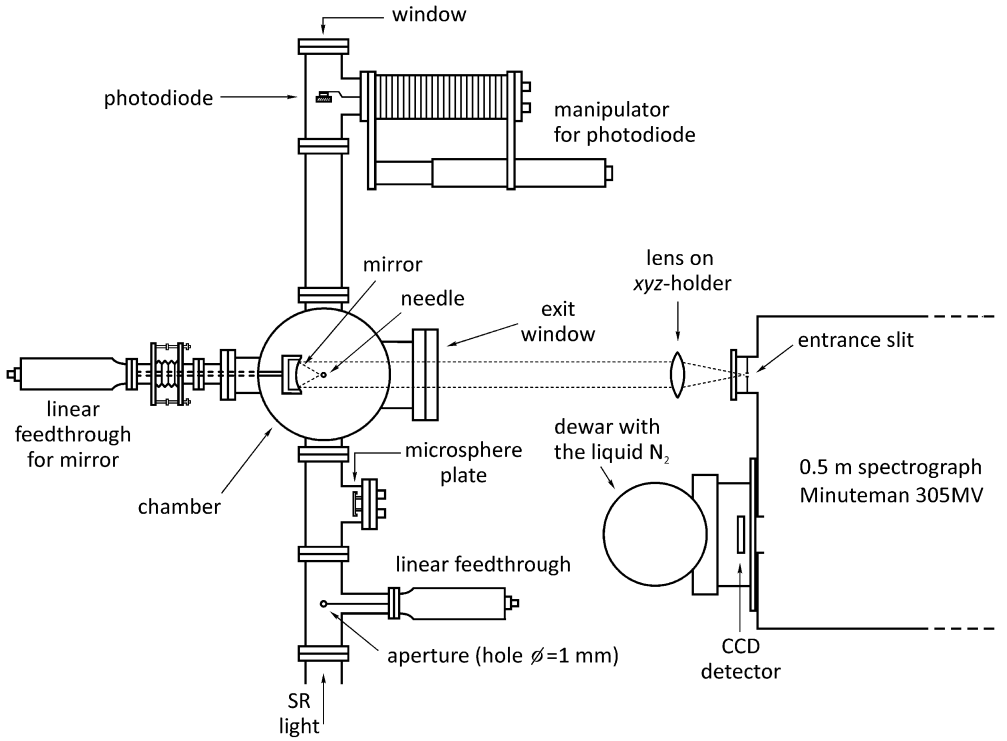

FIG. 2. Schematic view of the experimental system.

Two types of data were collected during the measurements. Fluorescence emission spectra were measured for a fixed incident photon energy with an optical resolution $\Delta\lambda$ in the spectrograph of 0.5 nm [full width at half maximum (FWHM)]. In a single data collection run, the CCD detector recorded fluorescence emission spectrum over a 40-nm wavelength range. The complete emission spectrum obtained in the 375–675 nm range consists of several 40-nm scans measured in different wavelength regions. The total exposure time for each 40 nm window was 30 min. The photodiode and photoion currents (photoion current from a microsphere plate, see Fig. 2) were simultaneously written in a log file together with the energy settings of the beamline and used in the normalization of the spectra. The wavelength scale was calibrated against the positions of the H_α to H_l lines of the Balmer series to within ± 0.1 nm. The background signal was measured by cutting off the incident synchrotron radiation and was subtracted from the fluorescence emission spectra. The obtained spectra were corrected for the wavelength dependence of the sensitivity of the optical detection channel.

The photodissociation efficiency curves were obtained by collecting fluorescence emission spectra over the selected 40-nm CCD window as a function of the incident photon energy. Measurements were performed using two different gratings. The low-energy grating operated in the photon energy range 13.6–20 eV with a step width of 100 or 150 meV, whereas the high-energy grating operated in the photon energy range 20–65 eV with a step width of 500 meV. The intensities of the emission lines observed in the fluorescence spectra were obtained by integrating over the peak areas. The intensity of fluorescence of the CH($A^2\Delta$) fragments includes vibrational and rotational bands. The background in the original spectra was taken to be the average of that below and above the studied lines and was subsequently subtracted from the spectra. The obtained fluorescence yields were normalized to the photon flux measured with a photodiode and corrected for sensitivity of the optical detection channel.

The detection efficiency of the experimental system in the 300–800 nm wavelength region was determined in a separate measurement using a source of monochromatized light. This was produced by a calibrated tungsten-halogen lamp attached to a fluorescence spectrograph (Acton Spectra Pro 300i). The monochromatized light at a given wavelength was introduced into the optical detection system using an optical fiber. Its end was placed at the exit window facing the Minuteman spectrograph. The intensity of light at each wavelength was recorded with the CCD detector in the first order of the spectrograph grating and was integrated over the line profiles. It was next normalized to the intensity of the incident light recorded with a calibrated photodiode (Newport 818-UV), whose output signal was measured by a Keithley 236 unit. Figure 3 presents the relative detection efficiency obtained as a function of detected wavelength. The highest contribution to the uncertainty of the efficiency curve comes from measurements of the photodiode current because it could not be measured simultaneously with the fluorescence spectra. The uncertainty in the measurements of the photodiode current was determined from variations between different readings. In the low-wavelength range (300–450 nm), this procedure gave an uncertainty of 20%. As expected, the detection efficiency peaks around 500 nm and in this wavelength region the uncertainty in the photodiode current measurement is less than 5%. In the remaining wavelength region, above 550 nm, it is 5–10%. In the above calibration procedure, the aluminum

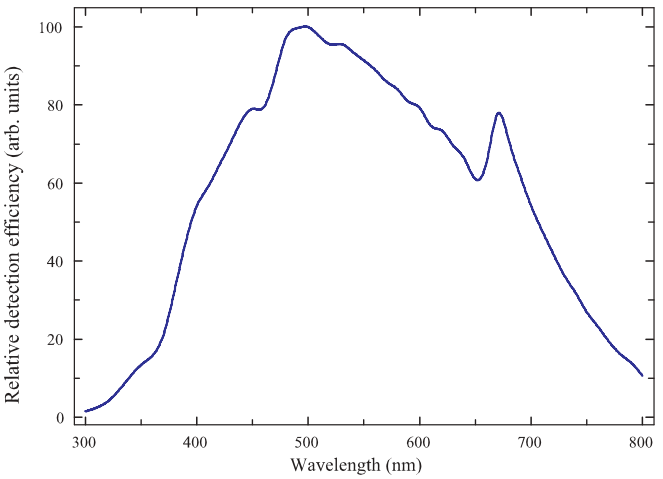

FIG. 3. (Color online) Relative detection efficiency of the experimental system determined in the 300–800 nm wavelength range.

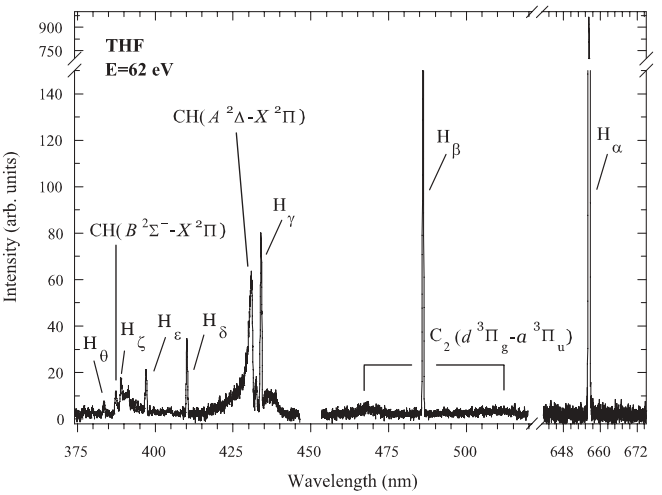

FIG. 4. Fluorescence emission spectrum measured for THF at a photon energy of 62 eV. The spectrum was corrected for the wavelength dependence of the sensitivity of the detection system.

spherical mirror that collimated the emitted fluorescence may alter the efficiency through wavelength dependence of its reflectivity. However, the reflectivity of Al in the wavelength range 200–1000 nm is quite constant (the difference between maximum and minimum does not exceed 6%) and on average its value is 86% [22]. We further note that the statistical uncertainty in the integration of the emission peaks is less than 1%. Taking into account the above contributions, we assign the total uncertainty in the relative detection efficiency of our optical channel to be 26%, 11%, and 16% in the 300–450 nm, 450–550 nm, and remaining wavelength region, respectively.

THF was purchased from Aldrich with a declared purity of 99.9% and was purified through freezing-pumping-thawing cycles until no further release of gases from the melting ices was observed. The THF vapor was directed through a gas inlet system and a hypodermic needle into the interaction region. The vapor pressure at room temperature was high enough that the gas-phase studies could be performed without heating the sample. The pressure in the vacuum chamber during the measurements had a typical value of 8×10^{-5} mbar while the pressure in the interaction region is estimated to be about 30 times higher than the ambient pressure.

III. RESULTS AND DISCUSSION

A. Fluorescence spectra

The fluorescence spectrum measured in tetrahydrofuran at a fixed photon energy of 62 eV and in the wavelength range 375–675 nm is shown in Fig. 4. This spectrum contains the hydrogen lines of the Balmer series, H_α to H_1, the $A^2\Delta \rightarrow X^2\Pi_r$ and $B^2\Sigma^- \rightarrow X^2\Pi_r$ emission bands of CH, and the much weaker $d^3\Pi_g \rightarrow a^3\Pi_u$ bands of the C_2 fragments. Figure 5 presents in detail the spectral region of the CH($A^2\Delta \rightarrow X^2\Pi_r$) bands, which extends from 413 to 445 nm. The shape of the CH profile arises from the overlapping series of rotational lines of the (0,0), (1,1), and (2,2) vibrational transitions. The positions of the lines are indicated in the figure following the spectroscopic measurements of Ref. [23]. The asymmetric peak at 431 nm arises from overlapping Q branches of the (0,0) and (1,1) vibrational transitions. The low-wavelength shoulder, below the peak, arises from overlapping R branches. The head of the Q branch of the (2,2) vibrational transition produces a low-intensity peak at 432.5 nm. The P branches of the vibrational transitions produce the structure above 433 nm, which is partly obscured by the H_γ line. The spectrum of Fig. 5 reveals high rotational excitation of the CH fragment up to $J = 34$. Figure 6 displays the spectral region covering the second band of CH($B^2\Sigma^- \rightarrow X^2\Pi_r$), which also contains the H_δ to H_1 lines of the Balmer series from H(n), $n = 6$–11. The CH emission band occurs between 387 and 409 nm and again shows high rotational excitation of this fragment up to $J = 20$, as indicated by the positions of the rotational lines ($\Delta v = 0$) taken from Ref. [23]. The bandhead of the R branch at 387 nm overlaps with the H_η line. The rotational lines produced by overlapping P and Q branches are affected by the H_ζ and H_ε hydrogen lines. The H_ζ line interferes with the bandheads of the P and Q

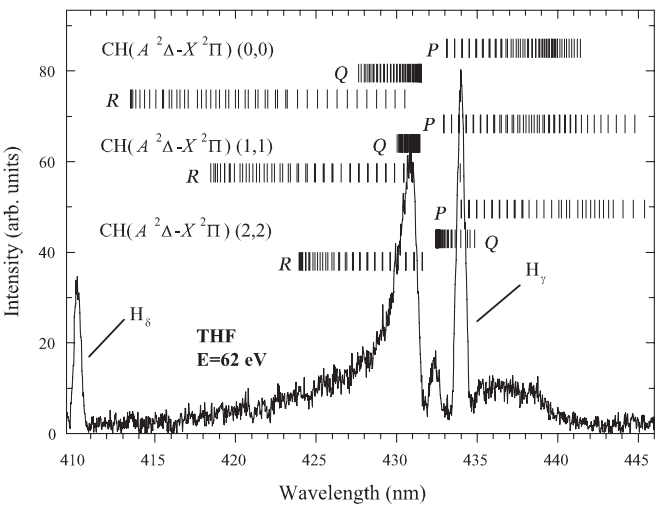

FIG. 5. Fluorescence emission spectrum of THF measured in the 410–445 nm wavelength range at a photon energy of 62 eV. The positions of the rotational lines of the Q, P, and R branches of the CH($A^2\Delta \rightarrow X^2\Pi_r$) bands are indicated by the vertical bars.

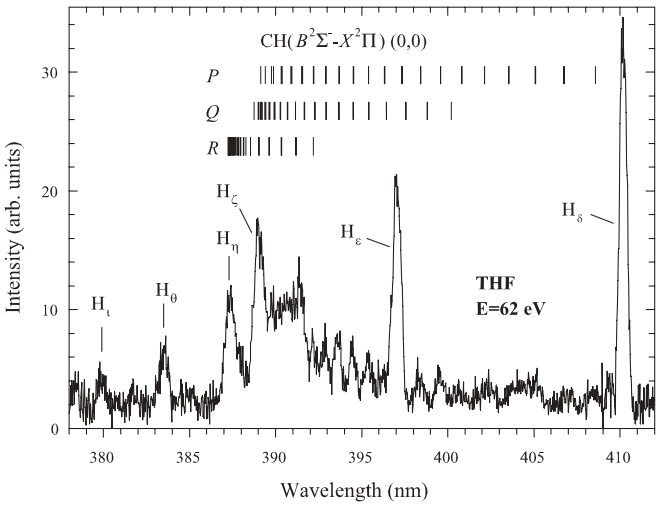

FIG. 6. Fluorescence emission spectrum of THF measured in the 380–410 nm wavelength range at a photon energy of 62 eV. The positions of the rotational lines of the Q, P, and R branches of the CH($B^2\Sigma^- \rightarrow X^2\Pi_r$) bands are indicated by the vertical bars.

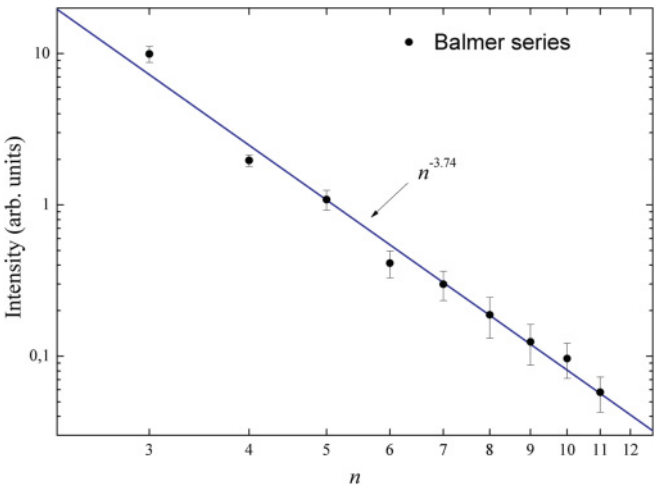

FIG. 8. (Color online) The emission intensity of the lines of the Balmer series as a function of the principal quantum number n. The solid line shows the best fit to the experimental points, which was obtained for an $n^{-3.74}$ dependence.

branches. Molecular $d^3\Pi_g \rightarrow a^3\Pi_u$ bands (Swan band) due to the vibrationally excited C_2, detected around 470 nm ($\Delta\upsilon = 1$) and 510 nm ($\Delta\upsilon = 0$), are presented in Fig. 7. Clearly discernible vibrational transitions are seen to originate from C_2, which is vibrationally excited up to $\upsilon = 6$ [24].

Figure 8 plots the intensity of the Balmer lines as a function of the principal quantum number n of the excited H(n) atoms. This dependence is approximated by a n^{-k} exponential function, where k is a constant. A least-squares fitting procedure gave $k = 3.74 \pm 0.25$. It is known that the intensities of the emission lines in the hydrogen series from (n,l) excited substates, populated according to their statistical weights ($2l + 1$), decrease with increasing n as n^{-3} to better than 5% [25]. This dependence was observed in electron impact dissociation of some heavier aliphatic hydrocarbons and silane for Balmer [26] and Lyman series [27], respectively. The present n dependence may be compared with that for dissociation of other five-membered ring molecules, furan [28], and isoxazole [29] studied using the electron impact optical excitation technique. These works, for the Balmer series, gave k values slightly higher than 3.0, 3.2 ± 0.3 and 3.57 ± 0.03, respectively. The above examples of ring molecules, including THF in the present work, demonstrate that the dissociation processes, which provide excited H(n,l) atoms, involve a number of higher-lying superexcited states which may be excited by electron impact or photoabsorption.

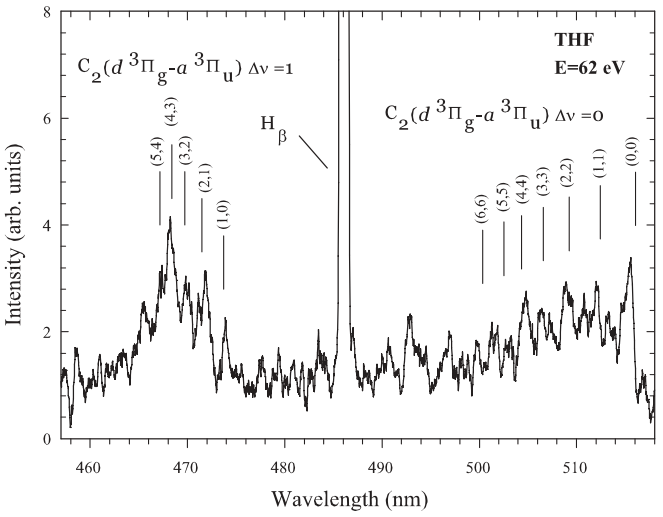

FIG. 7. Fluorescence emission spectrum of THF measured in the 460–515 nm wavelength range at a photon incident energy of 62 eV. The positions of the vibrational lines of the $C_2(d^3\Pi_g \rightarrow a^3\Pi_u)$ bands are indicated by the vertical bars.

B. Photodissociation efficiency curves

1. Excited hydrogen H(n) atoms

Dissociation efficiency curves for the production of H(n), n = 3–7, atoms measured in the 16.8–20 eV photon energy range by recording intensities of the Balmer H_α, H_β, H_γ, H_δ, and H_ϵ lines, respectively, are presented in Fig. 9. Each curve has the shape of a broad maximum with superimposed weak structure, which is most clearly seen in the $n = 4$ and 5 curves. These weak structures may indicate overlapping excitation bands of superexcited states. The $n = 3$ curve also has a shoulder on the low-energy side, which may correspond to a lower-lying superexcited state decaying preferably via the H($n = 3$) channel. The maxima of the curves shift to higher energies with increasing n value of the H(n) fragment. This behavior of the maxima may suggest that the corresponding superexcited states are Rydberg states of THF, THF(n_R), with the principal quantum number n_R. In this picture of THF dissociation, each of the excited THF(n_R) states in the dissociation process creates hydrogen atoms H(n). It is interesting to note that state-to-state neutral dissociation of Rydberg states, where the principal quantum numbers of the Rydberg orbitals of the molecules are the same as those of the excited atomic fragments, was previously observed in O_2 for states converging

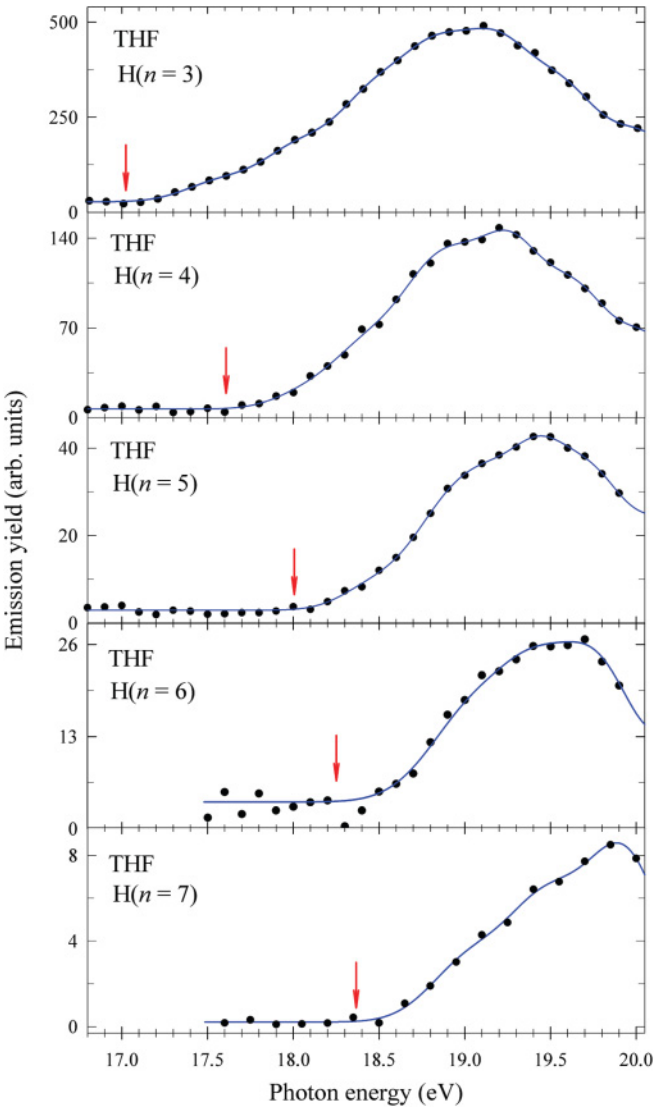

FIG. 9. (Color online) Dissociation efficiency curves for production of the H(n), $n = 3$–7, atoms measured in the 17–20 eV photon energy range. The (red) arrows indicate appearance energies of the fragments.

to the $c^4\,\Sigma_u^-$ state of O_2^+ [30]. The superexcited Rydberg states THF(n_R) would converge to the higher-lying $C_4H_8O^+$ ion state that constitutes the ion core. The recent threshold photoelectron spectra of THF [31] enable tentative identification of the ion core of these superexcited states to a strong, but so far unassigned, photoionization band with the vertical energy of 19.77 eV. This band occurs in the region of the 6a/4a″ and 4b/6a′ bands found in the theoretical calculations [32].

The AEs for the observed fragmentation processes were determined by fitting the dissociation efficiency curves of Fig. 9, in their threshold regions, with an exponential function which describes the energy dependence of the dissociation cross section [33]. The AEs obtained from the fitting procedure are indicated by arrows in Fig. 9 and are listed in Table I. Table I also compares the AEs with the estimated dissociation energy limits for direct elimination of the hydrogen H(n) atoms from the closed ring of THF. The estimated dissociation energy limit for H($n = 3$) is 16.06 eV. This value is obtained by

TABLE I. The appearance energies, dissociation energy limits, and the excitation energies (in eV) for the H(n), $n = 3$–7, and the CH($A^2\Delta$) fragments. The uncertainties of the appearance energies are determined from the fitting procedure.

Fragment	Appearance energy	Dissociation limit	Excitation energy
H($n = 3$)	17.0 ± 0.1	16.06	12.09
H($n = 4$)	17.6 ± 0.1	16.72	12.75
H($n = 5$)	18.0 ± 0.2	17.03	13.06
H($n = 6$)	18.2 ± 0.2	17.19	13.22
H($n = 7$)	18.3 ± 0.3	17.29	13.32
CH($A^2\Delta$)	14.9 ± 0.3	14.22	2.88

taking the excitation energy of the H($n = 3$) states, 12.09 eV, and the C-H bond strength of 3.97 ± 0.07 eV [34], which is in accord with the result of 3.88 eV (enthalpy at 0 K) from calculations of density functional theory [12]. The remaining dissociation limits were obtained using the corresponding excitation energies of the H(n) states, $n = 4$–7 (see Table I).

Alternative processes that may produce H(n) atoms would begin with cleavage of the C(2)-O(1) bond and formation of an excited intermediate diradical ·CH_2-CH_2-CH_2-CH_2-O·. Then, removal of an excited H(n) atom would occur on the potential energy surface corresponding to the excited state. The possible β-cleavage processes would involve H-atom abstraction from the C(5) atom accompanied by a simultaneous C(5)-O(1) π-bond formation or, but energetically less favorable, H-atom abstraction from the C(3) atom with formation of a C(2)-C(3) π bond. The dissociation energy limits of these two reactions have been estimated using the results of the calculations of Ref. [12] and are 16.25 and 16.82 eV, respectively. Other reactions that may produce H(n) atoms from the diradical require removal of a H atom from the C(2) or C(4) carbon atoms; however, these reactions have estimated dissociation energy limits that are above the presently measured AEs. It is of note that the measured AEs are greater by about 1 eV than the present estimations for the dissociation energy limits. This excess energy may appear in internal excitation of the ring and/or in the translational energy of the H(n) atom. For comparison, recent studies of electron impact fragmentation of THF molecules found a difference of 3.6 eV between the AE (19.7 ± 0.3 eV) of the H($n = 4$) channel and the estimated dissociation limit [35].

Figure 10 presents dissociation efficiency curves for H(n), $n = 3$–7, atoms measured in the 18–68 eV energy range with a 500 meV energy step. The first maxima, lying below 20 eV in each curve, are shown in detail in Fig. 9. The efficiency curves above 20 eV contain several bands, which were resolved by applying a fitting procedure with an appropriate number of Gaussian functions. The results of the fitting are shown in Fig. 10. The dissociation efficiency curves for the H(n) states have similar shapes and each curve was fitted with six bands [except for the H($n = 7$) curve, which was measured over a shorter energy range]. Good overall agreement with the measured spectra for $n = 3$–6, for that number of bands, is obtained. The vertical energies (centers) of the bands in the 22–24 eV region shift to higher energies with increasing n values, displaying a similar behavior to that observed for the bands lying below 20 eV. Thus, these bands may

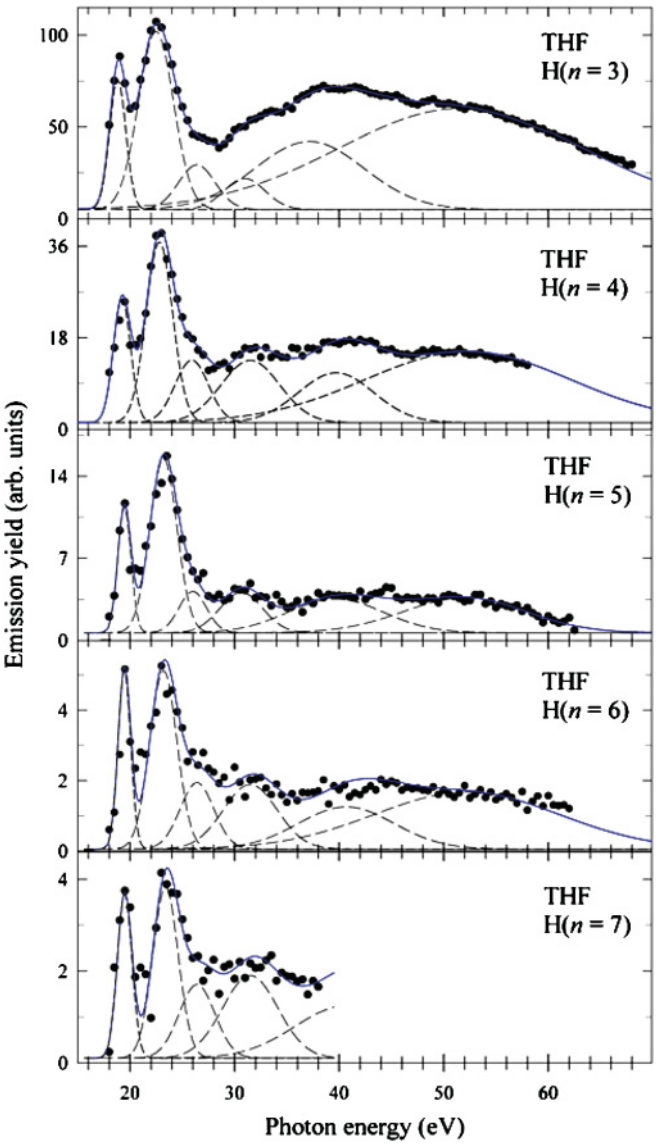

FIG. 10. (Color online) Dissociation efficiency curves for production of the H(n), n = 3–7, atoms measured in the 18–65 eV photon energy range. The bands fitted to the experimental curves are shown by the dashed lines and the final fits are shown by the solid lines.

correspond similarly to Rydberg superexcited states, which in this case may converge to the ionic states observed in the threshold photoelectron spectra at 23.23 and/or 24.36 eV [31]. The remaining bands occur at similar vertical energies in the dissociation efficiency curves for consecutive n values: the energies of the bands are found from the fitting procedure to lie within about 0.5 eV of each other. This suggests that these bands will be generated in each H(n) curve by the same superexcited state. The weighted mean vertical energies are listed in Table II. Higher widths of the three bands above 28 eV may impose that each of them contains a number of narrower bands, which, however, would be difficult to find from the fitting. The THF superexcited states above 28 eV would be built on deeper-lying ion cores and may correspond to doubly excited states. Superexcited states at higher energy may also decay by dissociative ionization.

TABLE II. The vertical energies (in eV) of the superexcited states of THF observed in the dissociation efficiency curves of the H(n), n = 3-7 atoms and the CH($A^2\Delta$) fragments in the 15-60 eV photon energy range. The uncertainties of the vertical energies are determined from the fitting procedure.

Energy	
H(n)	CH($A2\Delta$)
	15.3 ± 0.1
	16.5 ± 0.3
	18.48 ± 0.09
19.0–19.7	18.93 ± 0.12
	19.34 ± 0.10
	19.78 ± 0.10
22.5–23.4	22.1 ± 0.1
	24.0 ± 0.1
26.1 ± 0.1	26.5 ± 0.7
31.2 ± 0.2	31.4 ± 0.9
38.3 ± 0.3	40.0 ± 0.8
51.4 ± 1.0	49.0 ± 1.8

2. *Excited CH($A^2\Delta$) fragments*

Dissociation efficiency curves for excited CH($A^2\Delta$) fragments measured in the 14.6–20 and 20–60 eV energy regions, by detecting the $A^2\Delta \rightarrow X^2\Pi_r$ emission, are shown in Figs. 11 and 12, respectively. Both curves contain several bands, which overlap. To resolve these bands, a fitting procedure based on Gaussian functions was again applied. The broad peak between 18 and 20 eV in Fig. 11 displays structures that are attributed to vibrational bands of a superexcited state. These vibrational bands were fitted with four Gaussian peaks of equal width, which was found from the fitting to be 470 meV (FWHM). The energies determined for the centers of these bands are given in Table II. The average spacing between the

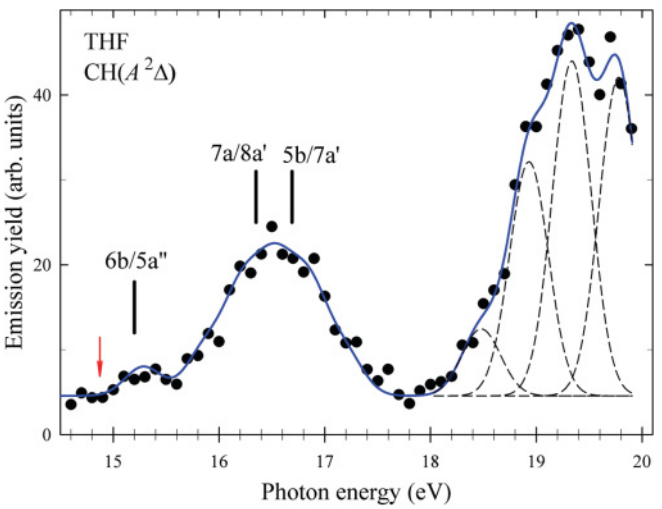

FIG. 11. (Color online) Dissociation efficiency curve for production of the CH ($A^2\Delta$) fragments measured in the 14.6–20 eV photon energy range. The bands fitted to the experimental curves are shown by the dashed lines and the final fit is shown by the solid line. The vertical bars show the positions of the photoionization 6b/5a″, 7a/8a′, and 5b/7a′ bands.

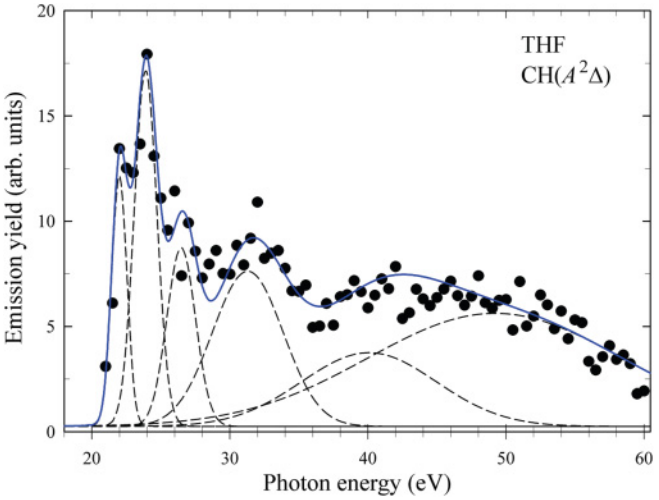

FIG. 12. (Color online) Dissociation efficiency curve for production of CH ($A^2\Delta$) fragments measured in the 20–60 eV photon energy range. The bands fitted to the experimental curves are shown by the dashed lines and the final fit is shown by the solid line.

vibrational bands is 0.43 eV and this value is comparable to the vibrational energy of 0.39 eV found in the calculations for the ν_1 CH_2 symmetric stretch mode of the ground ionic state of THF [36]. The broad peak between 18 and 20 eV and the resolved vibrational bands occur in the same energy region as the bands found in the H(n) efficiency curves (Fig. 9 and Table II). This overlap of the energy positions suggests that CH($A^2\Delta$) and H(n) fragments are formed by fragmentation of the same superexcited states. The efficiency curve above 20 eV (Fig. 12) could be fitted with six Gaussian profiles, which are considered to correspond to separate superexcited states. The results of this procedure are shown in Fig. 12 and the vertical energies of the fitted bands are listed in Table II. It is seen from Table II that these bands, except that at 24.0 eV, have corresponding counterparts in the dissociation efficiency curves of the H(n), $n = 3$–6, atoms, which clearly supports the interpretation of the superexcited states being the origin of the bands observed in both fragmentation channels. Two further broader bands centered at 15.3 and 16.5 eV are seen in the spectrum of Fig. 11. These bands appear below the AEs of the H(n) atoms and are not seen in their efficiency curves because of energetic reasons. The threshold photoelectron spectrum of THF shows photoionization 6b/5a″, 7a/8a′, and 5b/7a′ bands with vertical energies of 15.20, 16.35, and 16.69 eV, respectively [31], which coincide well with the energies of the centers of the broader bands, as indicated in Fig. 11. This may suggest that the corresponding superexcited states autoionize into the above ionic states with emission of threshold electrons in competition with the fragmentation process.

The AE of the CH($A^2\Delta$) fragment (Table I) was found to be 14.9 ± 0.3 eV. This value is lower than that obtained in electron impact studies of THF (18.9 ± 0.3 eV [35]). Formation of the CH($A^2\Delta$) fragment requires opening of the furanose ring of the THF molecule by breaking of the weakest C-O bond and further cleavage of the C(2)-C(3) bond (Fig. 1), leading to the final products of the reaction

$$C_4H_8O^* \rightarrow C_3H_6O + CH^*(A\,^2\Delta) + H. \quad (2)$$

The lowest fragmentation energy limit (Table I) for the above reaction is estimated to be 14.22 eV, as deduced from the following energies that are taken from known molecular dissociation data: the C(2)-O(1) bond cleavage, 3.14 eV [12]; breaking of the C(2)-C(3) bond, 3.81 eV [37]; and removal of the hydrogen atom from the CH_2, 4.39 ± 0.01 eV [38]. The excitation energy of the CH($A^2\Delta$) v = 0 level is 2.88 eV. Other possible processes leading to formation of the CH($A^2\Delta$) are, e.g.,

$$C_4H_8O^* \rightarrow C_3H_5O + CH^*(A\,^2\Delta) + H + H, \quad (3)$$

$$C_4H_8O^* \rightarrow C_3H_6 + CH^*(A\,^2\Delta) + H + O. \quad (4)$$

Process (3) would involve the C(2)-O(1) bond cleavage and next the C(2)-C(3) bond breakage with removal of the hydrogen atom from the CH_2 fragment, which may be further accompanied by a simultaneous H-atom abstraction from the C(5) carbon and C(5)-O(1) π-bond formation. The estimated fragmentation energy limit of the above reaction, 15.0 eV, is comparable to the measured AE of 14.9 ± 0.3 eV. It is of note that fragmentation processes, which involve cleavage of a higher number of bonds or formation of additional excited fragmentation species, have dissociation energy limits that are considerably higher than the measured AE. For example, for processes (4), which release propylene (C_3H_6) observed in the pyrolysis of THF [9], we estimate a dissociation energy limit of 18.2 eV.

IV. CONCLUSIONS

We have studied photofragmentation of THF molecules that produces excited atomic and molecular fragments using synchrotron radiation excitation. The following excited fragments have been observed in the photon energy range 14–68 eV: atomic hydrogen H(n), $n = 3$–11, the diatomic CH fragments in the $A^2\Delta$ and $B^2\Sigma^-$ states, and C_2 fragments in the $d^3\Pi_g$ state. The mechanism of the photofragmentation processes produces diatomic CH and C_2 species that are vibrationally and highly rotationally excited. The appearance energies of the H(n), $n = 3$–7, atoms and the CH($A^2\Delta$) radical were determined and compared with estimated fragmentation energy limits to discuss possible fragmentation processes. The fragmentation processes observed in THF induced by synchrotron radiation may be correlated with possible fragmentation of biomolecules which contain the furanose ring structure, for example purine nucleic acid bases, adenine and guanine.

ACKNOWLEDGMENTS

This work was carried out within COST Action CM0601, "Electron Controlled Chemical Lithography." It was supported by the Polish Ministry for Science and Higher Education under Contract No. 553/N-COST/2009/0. We thank E. Sovernigo for assistance in calibrating the efficiency of the fluorescence spectrograph. We are also grateful to the staff of the Synchrotron Trieste for assistance.

[1] A. L. Sobolewski, W. Domcke, C. Dedonder-Lardeux, and C. Jouvet, PhysChemChemPhys **4**, 1093 (2002).
[2] J. Wei, J. Riedel, A. Kuczmann, F. Renth, and F. Temps, Faraday Discuss. **127**, 267 (2004).
[3] M. Barbatti, M. Vazdar, A. J. A. Aquino, M. Eckert-Maksić, and H. Lischka, J. Chem. Phys. **125**, 164323 (2006).
[4] N. Gavrilov, S. Salzmann, and C. M. Marian, Chem. Phys. **349**, 269 (2008).
[5] S. Salzmann, M. Kleinschmidt, J. Tatchen, R. Weinkauf, and C. M. Marian, PhysChemChemPhys **10**, 380 (2008).
[6] R. Weinkauf, L. Lehr, E. W. Schlag, S. Salzmann, and C. M. Marian, PhysChemChemPhys **10**, 393 (2008).
[7] M. N. R. Ashfold, G. A. King, D. Murdock, M. G. D. Nix, T. A. A. Oliver, and A. G. Sage, PhysChemChemPhys **12**, 1218 (2010).
[8] C. H. Klute, and W. D. Walters, J. Am. Chem. Soc. **68**, 506 (1946).
[9] A. Lifshitz, M. Bidani, and S. Bidani, J. Phys. Chem. **90**, 3422 (1986).
[10] J. Kramer, J. Phys. Chem. **86**, 26 (1982).
[11] A. A. Scala and W. J. Rourke, J. Photochem. **37**, 281 (1987).
[12] A. A. Scala, E. W.-G. Diau, Z. H. Kim, and A. H. Zewail, J. Chem. Phys. **108**, 7933 (1998).
[13] S.-H. Lee, PhysChemChemPhys. **12**, 2655 (2010).
[14] S. SenGupta, H. P. Upadhyaya, A. Kumar, P. D. Naik, and P. Bajaj, J. Chem. Phys. **122**, 124309 (2005).
[15] M. Coreno, M. de Simone, M. Danailov, R. Richter, A. Kivimäki, M. Zitnik, and K. C. Prince, J. Electron Spectrosc. Relat. Phenom. **144–147**, 39 (2005).
[16] K. C. Prince *et al.*, J. Synchrotron Radiat. **5**, 565 (1998).
[17] K. Schulz, G. Kaindl, M. Domke, J. D. Bozek, P. A. Heimann, A. S. Schlachter, and J. M. Rost, Phys. Rev. Lett. **77**, 3086 (1996).
[18] K. Schulz, M. Domke, R. Püttner, A. Gutierrez, G. Kaindl, G. Miecznik, and C. H. Greene, Phys. Rev. A **54**, 3095 (1996).
[19] P. M. Dehmer, P. J. Miller, and W. A. Chupka, J. Chem. Phys. **80**, 1030 (1984).
[20] M. Zubek, G. C. King, and P. M. Rutter, J. Phys. B **21**, 3585 (1988).
[21] L.-E. Berg, P. Erman, E. Källne, S. Sorensen, and G. Sundström, Phys. Scr. **44**, 131 (1991).
[22] R. I. Solouchin, *Optics and Atomic Physics* (PWN, Warsaw, 1982).
[23] L. Gerö, Z. Phys. **118**, 27 (1941).
[24] C. V. V. Prasad, and P. F. Bernath, Astrophys. J. **426**, 812 (1994).
[25] H. A. Bethe and E. E. Salpeter, *Quantum Mechanics of One- and Two-Electron Atoms* (Plenum, New York, 1977), p. 267, Table 16a.
[26] J. M. Marendić, M. D. Tasić, and J. M. Kurepa, Chem. Phys. **91**, 273 (1984).
[27] S. Tsurubuchi, K. Motohashi, S. Matsuoka, and T. Arikawa, Chem. Phys. **155**, 401 (1991).
[28] M. Dampc and M. Zubek, Int. J. Mass Spectrom. **277**, 52 (2008).
[29] I. Linert, I. Lachowicz, T. J. Wasowicz, and M. Zubek, Chem. Phys. Lett. **498**, 27 (2010).
[30] M. Ukai, S. Machida, K. Kameta, M. Kitajima, N. Kouchi, Y. Hatano, and K. Ito, Phys. Rev. Lett. **74**, 239 (1995).
[31] M. Dampc, B. Mielewska, M. R. F. Siggel-King, G. C. King, and M. Zubek, Chem. Phys. **359**, 77 (2009).
[32] M. Yamauchi, H. Yamakado, and K. Ohno, J. Phys. Chem. A **101**, 6184 (1997).
[33] T. Fiegele *et al.*, Vacuum **63**, 561 (2001).
[34] F. R. Cruickshank and S. W. Benson, J. Am. Chem. Soc. **91**, 1289 (1969).
[35] M. Dampc and M. Zubek (unpublished).
[36] A. Giuliani, P. Limao-Vieira, D. Duflot, A. R. Milosavljevic, B. P. Marinkovic, S. V. Hoffmann, N. Mason, J. Delwiche, and M.-J. Hubin-Franskin, Eur. Phys. J. D **51**, 97 (2009).
[37] D. R. Lide (Ed.), *CRC Handbook of Chemistry and Physics* (CRC Press, Boca Raton, FL, 2004).
[38] S. J. Blanksby and G. B. Ellison, Acc. Chem. Res. **36**, 255 (2003).